48th AIAA/ASME/SAE/ASEE Joint Propulsion Conference & Exhibit
30 July - 01 August 2012, Atlanta, Georgia

AIAA 2012-4336



# Performance of a Helicon Hall Thruster Operating with Xenon, Argon, and Nitrogen

Adam Shabshelowitz[1] and Alec D. Gallimore[2]
*The University of Michigan, Ann Arbor, MI, 48105, USA*

*and*

Peter Y. Peterson[3]
*ElectroDynamic Applications, Inc., Ann Arbor, MI, 48105, USA*

**The Helicon Hall Thruster (HHT) is a two-stage thruster that was developed to investigate whether a radiofrequency ionization stage can improve the overall efficiency of a Hall thruster operating at high thrust and low specific impulse. This experiment measured the single-stage and two-stage performance of the HHT for 10-25 mg/s anode mass flow rates of xenon at 100-200 V discharge voltages, and also for 6 mg/s of argon at 300 V, and 2.6 mg/s of nitrogen at 200 V. Argon and nitrogen performance are characterized by low beam divergence efficiency and low propellant utilization efficiency. During two-stage operation, the thrust of the HHT increased slightly with rf power, but the propulsive efficiency and thrust-to-power both decreased with increasing rf power. Probe diagnostics suggest that gains were realized by a slight increase in propellant efficiency, but that the rate of increase was not sufficient to overcome the increase in power.**

## Nomenclature

| | | |
|---|---|---|
| $A_{c,eff}$ | = | Faraday probe effective collection area [m$^2$] |
| $e$ | = | elementary charge [C] |
| $E_1$ | = | voltage exchange parameter [-] |
| $E_2$ | = | mass exchange parameter [-] |
| $\mathcal{F}$ | = | Faraday constant [C/mol] |
| $I_{axial}$ | = | axial component of ion beam current [A] |
| $I_{beam}$ | = | ion beam current [A] |
| $I_c$ | = | current collected by probe [A] |
| $I_d$ | = | discharge current [A] |
| $I_{sp,a}$ | = | anode specific impulse [s] |
| $I_{sp,a}^{+}$ | = | theoretical anode specific impulse of a singly-charged plasma [s] |
| $\mathcal{M}$ | = | molar mass [kg/mol] |
| $m_i$ | = | ion mass [kg] |
| $\dot{m}$ | = | total thruster mass flow rate [kg/s] |
| $\dot{m}_a$ | = | anode mass flow rate [kg/s] |
| $\dot{m}_c$ | = | cathode mass flow rate [kg/s] |
| $P_d$ | = | discharge power [W] |
| $P_{elec}$ | = | total electrical power [W] |
| $P_{dc}$ | = | dc discharge power $\equiv I_d V_d$ [W] |
| $P_{mag}$ | = | magnet power [W] |
| $P_{rf}$ | = | rf power [W] |
| $P_{thrust}$ | = | jet power of thruster exhaust [W] |

[1] Graduate Student Research Assistant, Department of Aerospace Engineering, Member AIAA.
[2] Arthur F. Thurnau Professor, Department of Aerospace Engineering, Fellow AIAA.
[3] Currently at Aerojet in Redmond, WA, Member AIAA.

| | | |
|---|---|---|
| $r$ | = | Faraday probe distance from thruster [m] |
| $T$ | = | measured thrust [N] |
| $T^{+}$ | = | theoretical thrust of a thruster with singly-charged plasma [N] |
| $v_{axial}$ | = | average axial velocity of exhaust particle [m/s] |
| $V_d$ | = | discharge voltage [V] |
| $V_{mp}$ | = | most probable energy of exhaust ions [V] |
| $V_p$ | = | plasma potential [V] |
| $\eta_a$ | = | anode efficiency [-] |
| $\eta_a^+$ | = | anode efficiency of a thruster with singly-charged plasma [-] |
| $\eta_c$ | = | cathode efficiency [-] |
| $\eta_d$ | = | discharge efficiency $\equiv \eta_a \eta_c \eta_{rf}$ [-] |
| $\eta_{mag}$ | = | magnet power efficiency [-] |
| $\eta_I$ | = | current utilization efficiency [-] |
| $\eta_{rf}$ | = | rf power efficiency [-] |
| $\eta_t$ | = | total efficiency [-] |
| $\eta_V$ | = | voltage utilization efficiency [-] |
| $\theta$ | = | angular position of Faraday probe [radians] |
| $\lambda$ | = | effective exhaust divergence angle [degrees] |
| $\Phi_P$ | = | propellant utilization efficiency [-] |
| $\Psi_B$ | = | beam divergence efficiency [-] |

## I. Introduction

HALL thrusters were first employed in space by the former Soviet Union in the 1970's, but it was not until the early 1990's that significant Hall thruster development work occurred in the United States.[1] Current Hall thruster research activities primarily focus on improving thruster lifetime,[2] using propellants other than the traditional xenon,[3,4] increasing the power and thrust density,[5,6] and extending the range of performance.[7,8] The success seen by many of these research efforts show that Hall thrusters are a robust and versatile technology.

Helicon plasma sources have been studied since the 1960's, with early studies focusing on their ability to efficiently produce high-density plasma for materials processing.[9,10] Since that time, a considerable amount of development work toward using helicon sources in electric propulsion systems has been performed. Some of this work involves the use of a helicon source alone as a thruster,[11-14] while other propulsion systems attempt to use the helicon source as an ionization stage, with a separate acceleration stage.[15-17] Previous work has also demonstrated the operation of an annular helicon source, which may be applied as an ionization stage for a two-stage Hall thruster.[18]

The Helicon Hall thruster (HHT) is a two-stage thruster designed to utilize the efficient ionization of a helicon plasma source with the acceleration mechanism of a Hall thruster. In particular, HHT was constructed to investigate whether the inclusion of a radiofrequency (rf) ionization stage could increase the overall efficiency of a Hall thruster operating in a high thrust-to-power, low specific impulse operating regime. The performance of the HHT was measured in the University of Michigan's Plasmadynamics and Electric Propulsion Laboratory (PEPL) during the summer of 2010, and the results showed a trend that suggested performance could be improved when higher levels of rf power were used.[19] A follow-on study was performed during the summer of 2011 with an improved rf power delivery system and thrust stand electromagnetic interference (EMI) mitigation scheme to confirm the results from 2010. During the follow-on test, the performance of the HHT operating with argon and nitrogen propellant was also measured. This report presents the results of the follow-on test.

## II. Methodology

There are many ways to break down the total efficiency of a Hall thruster into component quantities.[1,20] These components are determined by thruster telemetry, performance measurements, and probe diagnostics, and they can reveal the physical nature of thruster inefficiencies. This section outlines the efficiency architecture used to evaluate the performance of the HHT.

### A. Single-stage efficiency

The total efficiency of a thruster is simply the power of the thrust-producing component of the exhaust divided by the total electrical power consumed by the thruster, as presented in Eq. 1. In laboratory-model Hall thrusters, such as the HHT, the magnetic circuit design is generally not optimized for power consumption, and so the magnet power efficiency is separated accordingly. In addition, the cathode is not always optimized as it would be on a flight model thruster, so the cathode effects are also separated. The results of this breakdown allow the discharge or anode efficiency to be individually examined, as shown in Eq. 2.

$$\eta_t = \frac{P_{thrust}}{P_{elec}} = \frac{\frac{1}{2}\dot{m}v_{axial}^2}{P_d + P_{mag}} \tag{1}$$

$$\eta_t = \frac{\frac{1}{2}\dot{m}_a v_{axial}^2}{P_d}\left(1 + \frac{\dot{m}_c}{\dot{m}_a}\right)\frac{1}{\left(1 + \frac{P_{mag}}{P_d}\right)} = \eta_a \eta_c \eta_{mag} = \eta_d \eta_{mag} \tag{2}$$

Brown et al. suggest that using the "voltage exchange parameter," $E_1$, and the "mass exchange parameter," $E_2$, can help elucidate the physical sources of inefficiency using only thruster telemetry and thrust measurements, as represented in Eq. 3.[20] Any further efficiency analysis requires the use of probe diagnostics.

$$\eta_d = E_1 E_2 = \left[\frac{\frac{1}{2}\left(T/\dot{m}\right)^2}{V_d\left(\mathcal{F}/\mathcal{M}\right)}\right]\left[\frac{\dot{m}\mathcal{F}}{I_d \mathcal{M}}\right] = [\Phi_P \Psi_B \eta_V][\eta_I] \tag{3}$$

### B. Two-stage efficiency

The difference between single-stage and two-stage operation is that two-stage operation uses rf power to affect the discharge in the vicinity of the gas inlet manifold. The way that this can be accounted for in the efficiency architecture is shown below in Eq. 4.

$$\eta_d = \frac{\frac{1}{2}\dot{m}_a v_{axial}^2}{P_{dc} + P_{rf}}\eta_c = \eta_a \frac{1}{\left(1 + \frac{P_{rf}}{P_{dc}}\right)}\eta_c = \eta_a \eta_{rf} \eta_c \tag{4}$$

This definition of rf efficiency is consistent with the single-stage architecture, since $\eta_{rf} = 1$ when no rf power is used. It also allows the exchange parameters to retain their original definition in Eq. 3. This allows the effect of the rf power on the thruster performance characteristics to be examined through the exchange parameters. In order to evaluate the net effect of rf power on propulsive efficiency, however, the rf efficiency must also be included.

## III. Apparatus

This experiment was performed in the Large Vacuum Test Facility (LVTF) at PEPL. The LVTF is a 6-meter diameter by 9-meter long cylindrical, stainless-clad steel chamber. Seven CVI TM-1200 nude cryopumps evacuate the LVTF at a combined pumping speed of 500,000 Liters per second on air or 245,000 Liters per second on xenon. The probe diagnostics discussed below have all been previously used to characterize Hall thrusters at PEPL.[1,21]

### A. Thruster

The HHT is a two-stage thruster, with an rf ionization first stage and a Hall acceleration second stage. In the first stage, a loop antenna is employed along with a strong axial magnetic field just downstream of the propellant distributor. The axial magnetic field and loop antenna are designed to excite annular helicon wave modes in the first part of the discharge channel. The second stage uses a radial magnetic field and auxiliary electrodes with an external cathode to create a traditional Hall accelerator. During this follow-on test, the auxiliary electrodes were not in place, and the propellant distributor is used as the Hall accelerator anode. For more detailed discussions regarding the HHT design, the reader is referred to Martinez et al.[7] and Peterson, et al.[19]

### B. RF power system

A Comdel CPS-3000 rf generator supplies rf power at a fixed frequency of 13.56 MHz. The CPS-3000 has a maximum output power of 3000 W and a standard 50-Ω output, and it is designed to tolerate high amounts of reflected power. An RG-213 coaxial cable transmits rf power from the CPS-3000 output port to a hermetically sealed, HN-type bulkhead connector at the LVTF wall that acts as a vacuum feedthrough. Inside the LVTF, an RG-393 coaxial cable transmits the rf power from the feedthrough to the thrust stand platform. The final connection to the HHT matching network is made using a shorter length of RG-393 coaxial cable, and it is arranged to minimize forces on the thrust stand due to thermal expansion of the cable. Thus, a 50-Ω system is maintained from the rf generator to the HHT matching network on the thrust stand.

The matching network is installed in the vacuum chamber to minimize the physical distance between the matching network output and the HHT antenna leads, and to increase the likelihood that the rf power measurements represent the actual power that is being delivered to the plasma. The matching network is in an L-type configuration, and two dc motors turn the two vacuum variable capacitors. The dc motors are manually controlled from outside the vacuum chamber by using a tethered remote-control box.

A Werlatone -60 dB dual-directional coupler rated to 10 kW of power at 2-32 MHz (Model# C5389-32) is used to determine the rf power in the system. The directional coupler's frequency response is calibrated and shown to be a constant -60 dB over the range of 1-60 MHz using an Agilent E5071C network analyzer. Directivity for both the forward and reflected coupling port is a constant -30 dB over the same frequency range. The dual-directional coupler was placed in the vacuum chamber and connected directly in-line at the matching network rf power input port. The forward and reflected voltage signals are observed both with an Agilent DSOX3024A oscilloscope and with a spectrum analyzer to monitor the health and general behavior of the rf power delivery system. For each data point employing rf power, the oscilloscope records 2 ms of forward and reflected voltage waveform data sampled at 2 GSa/s, and post-processing is used to determine the forward and reflected power.



### C. Thrust stand

The inverted pendulum, null-type thrust stand at PEPL is very similar to that described by Xu and Walker,[22] except there is no piezoelectric control of the inclination. During this experiment, the thrust stand is operated in displacement mode in order to allow a simple and reliable check for EMI. In displacement mode, an electromagnetic damper coil eliminates high-frequency oscillations in the position of the thrust stand, and a steady thrust displaces the equilibrium position.

The EMI check is as follows: the thrust stand spring is replaced by a solid bar of mica material, so that the thrust stand equilibrium position is locked in one place. The thruster is then operated normally with and without rf power, and if any change in the position is observed during operation, the change is noted to be a result of EMI. Although the unmodified experimental setup exhibited signs of EMI, including increased noise and dc offsets on telemetry and performance signals, the effect of the rf plasma on the thrust stand was eventually eliminated by implementing an EMI mitigation scheme similar to that described by Kiekhafer and Walker.[23] Observations in this experiment indicated that the most effective reduction of EMI occurred with the application of split-core ferrite beads to all electrical cables leading to the thruster and thrust stand. It is extremely important, however, that the proper "mix" of ferrite material is chosen so that the impedance of each electrical cable is maximized at the rf driving frequency.

### D. Faraday Probe

A nude Faraday probe was used to measure the ion current density in the HHT exhaust plume. This Faraday probe is described in detail by Liang and Gallimore,[21] and is modeled after the nested Faraday probe design described by Brown and Gallimore.[24] The Faraday probe was mounted to a rotation stage such that it could move in an arc about the HHT exit plane. To take data, the guard ring and both collectors are biased at -30 V with respect to facility ground into ion saturation. The current drawn by the inner collector is recorded as the probe is swept between -90 and 90 degrees, where 0 degrees is along the thruster centerline.

The total ion beam current is calculated from Eq. 5, where the effective collector area includes all correction factors described by Brown.[25] The axial beam current is calculated from Eq. 6, and an effective exhaust divergence angle is calculated according to Eq. 7. Following from the efficiency architecture of Brown et al., the beam divergence efficiency is defined in Eq. 8.[20]

$$I_{beam} = 2\pi r^2 \int_0^{\pi/2} \frac{I_c(\theta)}{A_{c,eff}} \sin(\theta)\, d\theta \tag{5}$$

$$I_{axial} = 2\pi r^2 \int_0^{\pi/2} \frac{I_c(\theta)}{A_{c,eff}} \sin(\theta)\cos(\theta)\, d\theta \tag{6}$$

$$\lambda = \cos^{-1}\left(\frac{I_{axial}}{I_{beam}}\right) \tag{7}$$

$$\Psi_B = \left(\frac{I_{axial}}{I_{beam}}\right)^2 \tag{8}$$

### E. Retarding Potential Analyzer

The ion voltage distribution (IVD) is measured with a retarding potential analyzer (RPA) that has been previously used to measure plasma properties in a helicon plasma source at PEPL,[26] as well as other Hall thrusters.[1,5] The RPA is based on a design by the Air Force Research Laboratory, and is described in detail by Hofer.[1] It consists of three grids and a collector contained in a stainless steel case. The grids and collector are isolated from each other and the case by macor spacers. The floating grid first accepts charged particles from the plasma in a minimally disruptive manner. The electron repelling grid is biased to a constant -30 V potential with respect to facility ground, which prevents incident electrons from reaching the collector. The ion retarding grid is swept from 0 to 500 V above ground with a Keithley 2410 SourceMeter to progressively filter out higher-energy ions. A Keithley 6485 Picoammeter measures the current to the collector at each ion retarding voltage, and the IVD is directly proportional to the first derivative of the measured current-voltage characteristic. The ion retarding grid voltage at which the maximum in the IVD occurs is the "most probable ion energy," $V_{mp}$, and is used to determine the voltage utilization efficiency.

The RPA is mounted to a linear translation stage with the floating grid located approximately 6 meters downstream of the thruster exit plane. A Langmuir probe is also mounted to the translation stage so that both RPA and Langmuir probe data could be taken at the same position. The plasma potential, $V_p$, is taken as the peak in the first derivative of the Langmuir probe current-voltage characteristic, and the voltage utilization efficiency is calculated from the RPA and Langmuir probe data according to Eq. 9.

$$\eta_V = \frac{V_{mp} - V_p}{V_d} \tag{9}$$

## IV. Results

The performance of the HHT was measured on xenon, argon, and nitrogen propellants with and without the rf stage operating. When operating with argon and nitrogen, research grade xenon was used for cathode flow. The HHT was constructed to investigate whether an rf ionization stage could increase the efficiency of a Hall thtruster operating in a low-specific impulse regime, and so this experiment mainly focused on low discharge voltage operating conditions. Table 1 summarizes the HHT operating conditions and plume measurements that were analyzed during this experiment, with the "Plume Measurements" column indicating when probes were used to make measurements in single-stage mode or while the rf stage was operating. Single-stage performance results are presented in this section first, followed by single-stage probe measurements, and then two-stage performance and probe results.

### A. Single-Stage Operation

Results of the HHT single-stage performance test are shown in Figs. 1 and 2. Figure 1 shows the expected result that anode specific impulse increases with discharge voltage, and thrust increases with both discharge voltage and anode mass flow rate, regardless of the propellant used. Figure 2 shows that the thrust-to-power (T/P) for the HHT operating with xenon is between 60 mN/kW and 72 mN/kW. When operating with xenon propellant, both anode efficiency and T/P tend to increase with increasing discharge voltage, and are maximized at the intermediate anode mass flow rates. Although argon and nitrogen operating conditions were at higher discharge voltages, T/P is only 30 mN/kW and 21 mN/kW, and anode efficiency is 29% and 15%, respectively.

In order to investigate the potential sources of inefficiency when using alternate propellants, the exchange parameters described above in Section II are plotted as a function of anode mass flow rate. The exchange parameters are only a function of performance measurements and thruster telemetry, and therefore do not require any probe results. Note that the cathode flow was xenon, and so the average molar mass of the cathode and anode propellant flow is used in the exchange parameter calculations.

**Table 1 Summary of HHT operating conditions**

| Propellant | Anode Flow Rate (mg/s) | Discharge Voltage (V) | RF Power Range (W) | Cathode Flow Fraction | Plume Measurements* |
|---|---|---|---|---|---|
| xenon | 10.0 | 200 | 0 – 1036 | 7.1% | 1s |
| xenon | 14.9 | 100 | 0 – 1028 | 5.0% | 1s |
| xenon | 14.9 | 150 | 0 – 1041 | 5.0% | 1s |
| xenon | 14.9 | 200 | 0 – 1032 | 5.0% | 1s |
| xenon | 20.0 | 100 | 0 – 994 | 5.0% | 1s & 2s |
| xenon | 20.0 | 150 | 0 – 1205 | 5.0% | 1s & 2s |
| xenon | 20.0 | 200 | 0 – 986 | 5.0% | 1s |
| xenon | 25.0 | 200 | 0 – 613 | 7.0% | - |
| argon | 5.95 | 300 | 0 – 270 | **16.8% | 1s & 2s |
| nitrogen | 2.60 | 200 | 0 – 302 | **38.4% | 1s |

*1s = single-stage operation, 2s = two-stage operation
**cathode flow was set to 1.0 mg/s of xenon for argon and nitrogen operating conditions

The exchange parameters are plotted in Fig. 3 versus anode mass flow rate. Figure 3(a) shows that $E_1$ increases with anode mass flow rate and voltage. Although the nitrogen and argon operating conditions were at relatively higher voltages, $E_1$ remained fairly low, comparable to the 100-V, 15-mg/s xenon case. It appears that the nitrogen operating point follows the trend for 200-V operation with xenon, and that it may simply be the low mass flow rate that explains the low value of $E_1$. However, the argon point appears that it may have a lower $E_1$ than would a 300-V operating condition with an equivalent xenon mass flow rate. Figure 3(b) shows that $E_2$ for xenon operation decreases with anode mass flow rate, and is not significantly affected by discharge voltage. In contrast to $E_1$, $E_2$ for argon appears to follow the trend for xenon, whereas $E_2$ for nitrogen is much lower; however, it is unclear whether or not the behavior of a xenon operating point with an equivalently low anode mass flow rate would follow the nitrogen results. In either case, Eq. 3 shows that $E_2$ has the same definition as current utilization in the efficiency architecture used here, and so the low anode efficiency of the nitrogen operating point is partly explained by a low current utilization.

A nude Faraday probe is used to measure the current density in the exhaust plume. Typically, the total thruster ion beam current is determined by assuming axisymmetry according to Eq. 5. The resulting beam current can be used to determine the mass utilization efficiency. The Faraday probe data from this experiment yielded mass utilization

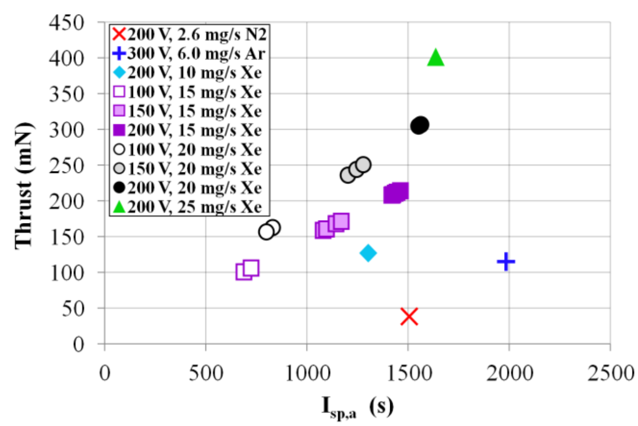


**Figure 1. Single-stage thrust versus specific impulse.**

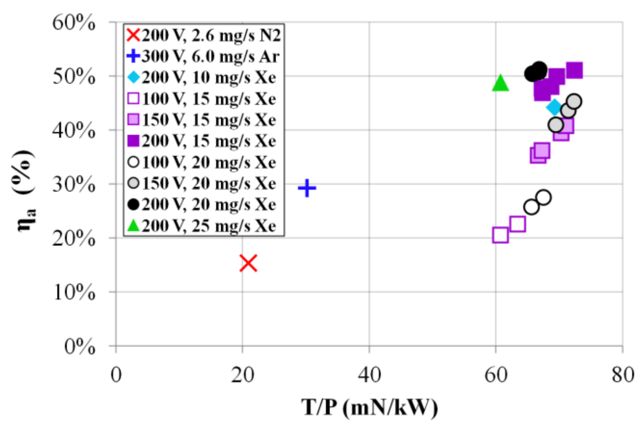


**Figure 2. Single-stage anode efficiency versus thrust-to-power.**

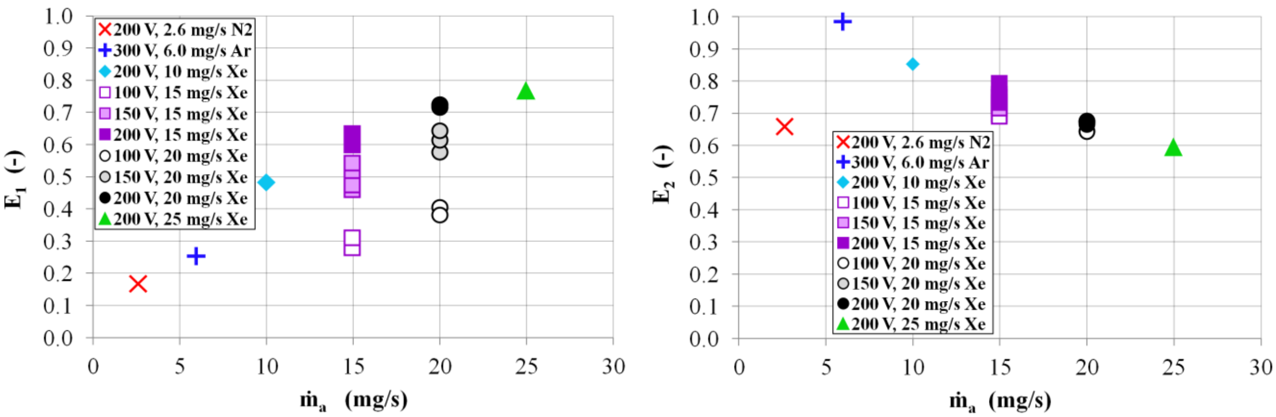


**(a)** **(b)**

**Figure 3. Exchange parameters plotted versus anode mass flow rate.**

results that were unphysical (greater than 100%), and so they are not reported here. The beam divergence efficiency is not as sensitive to the absolute integrated values of total and axial beam current, and so those results are reported in Fig. 4. Previous results have shown that beam divergence efficiency increases with increasing discharge voltage, and weakly increases with increasing anode flow rate;[20] however, these results show that the beam divergence of the 200-V nitrogen condition is equivalent to the 100-V xenon conditions, and the divergence of the 300-V argon condition is nearly the same as the 150-V xenon conditions. This result shows that the beam divergence efficiency is affected by propellant gas species, and not simply mass flow rate.

This finding is consistent with the results seen by Linell,[27] who showed that krypton propellant consistently had a lower beam divergence efficiency than xenon for equivalent operating conditions in the NASA-173Mv1. Although the beam divergence efficiency is lower for the nitrogen and argon operating points, divergence alone does not completely explain the lower values of $E_1$ seen in both (and in the 100-V xenon operating points, for that matter).

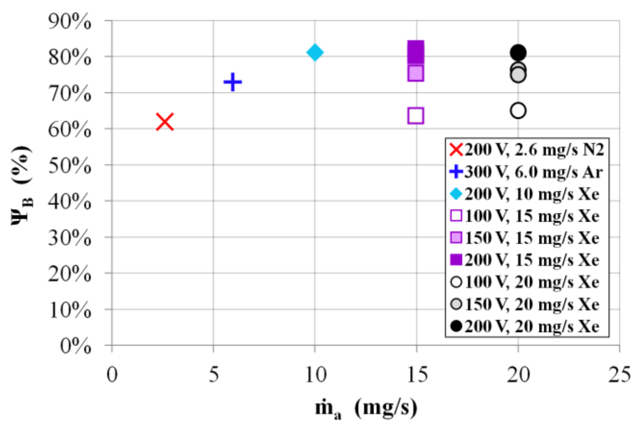


**Figure 4. Beam divergence efficiency from Faraday probe data.**

The RPA and Langmuir probe are used to determine the voltage utilization efficiency. The results are plotted in Fig. 5, which shows that argon and nitrogen voltage utilization efficiency does not have a significant deficit compared to xenon. The nitrogen operating point appears to fall in line with the 200-V xenon trend, and the slightly higher voltage utilization of the argon operating point is simply explained by the fact that voltage utilization tends to increase with increasing discharge voltage. Discharge voltage therefore remains the dominant factor in determining voltage utilization, further evidenced by the lower voltage utilization of the 100-V xenon operating points.

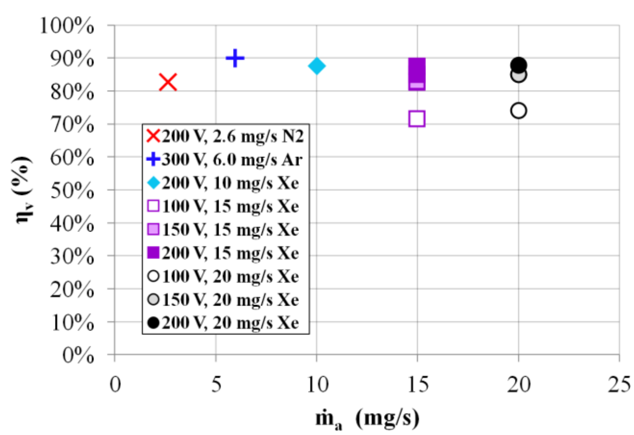


**Figure 5. Voltage utilization from RPA and Langmuir probe data.**

Taking the results from Figs. 3-5 with Eq. 3, the deduction is readily made that a lower propellant utilization for nitrogen and argon can explain the lower anode efficiency. This conclusion again agrees with the results seen by Linell, who states that “the beam divergence accounts for a loss equally important as propellant utilization" when referring to operation with krypton versus xenon propellant.[27] An interesting observation is that diatomic nitrogen and argon have nearly the same first ionization energy, 15.58 eV and 15.76 eV, respectively, compared to 12.13 eV for xenon.[28] Despite the fact that rotational and vibrational energy modes can sink energy away from a nitrogen discharge and not an argon one, no significant difference in voltage utilization or propellant utilization is seen. Rather, the major difference in anode efficiency between argon and nitrogen is explained by the fact that current utilization for nitrogen is much lower than that of argon.

In order to investigate whether the lower performance observed for argon and nitrogen propellant might be explained purely by those propellant species' lower molar masses, the semi-empirical thrust of a thruster with a singly-charged plasma is determined using thruster telemetry and probe results with Eq. 10. The theoretical performance is plotted in Figs. 6 and 7. Comparing the theoretical results to the measured performance plotted in Figs. 1 and 2, the theory most accurately reproduces the xenon results at 15 mg/s anode flow rate and the nitrogen operating point. Equation 10 under predicts xenon performance at 20 mg/s, slightly over predicts xenon performance at 10 mg/s, and significantly over predicts HHT performance at the argon operating point. The results suggest that HHT performance with nitrogen at 200 V is well described by the theory, but since Eq. 10 only applies for a singly-charged plasma, they also suggest that there may be some additional performance losses and gains due to multiply-charged species for the argon operating point.

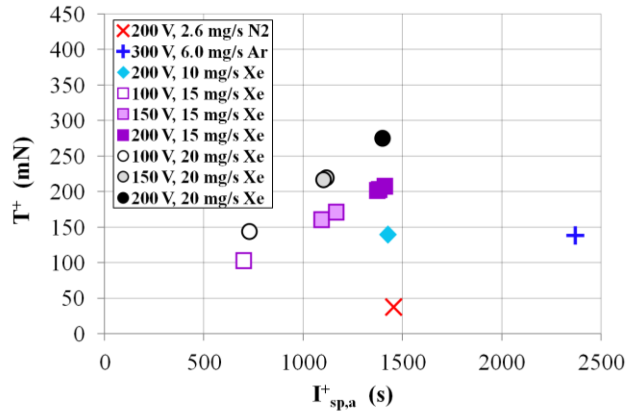


**Figure 6. Theoretical thrust versus specific impulse.**

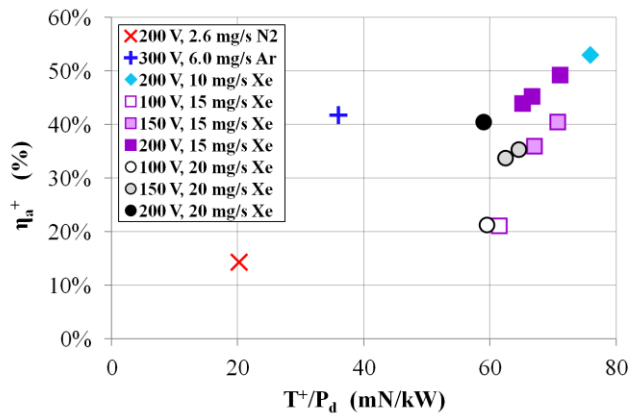


**Figure 7. Theoretical efficiency and thrust-to-power.**

$$T^{+} = \Psi_B \eta_I I_d \sqrt{\frac{2 m_i V_d \eta_V}{e}} \tag{10}$$

## B. Two-stage operation

During two-stage operation, the rf ionization stage was powered in the attempt to increase HHT anode efficiency at high thrust-to-power (T/P) operating points. The magnets in the helicon section were held constant as rf power was increased, since it was seen that the magnets for the helicon stage could act as trim coils for the Hall stage when no rf power was used. Figure 8 shows that thrust increased slightly with rf power on for most operating conditions; however, Fig. 9 shows that the rate of increase in thrust is always exceeded by the rate of increase in rf power, such that the overall T/P decreases with increasing rf power. The decreasing trend with rf power is also observed in the total anode efficiency, which includes rf efficiency, as shown in

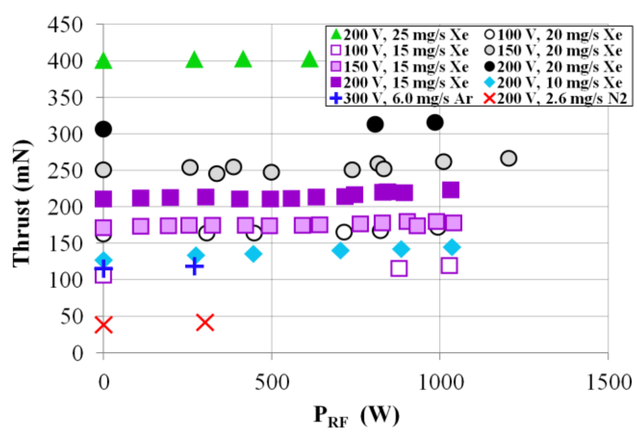


**Figure 8. Two-stage thrust versus rf power.**

Fig. 10.

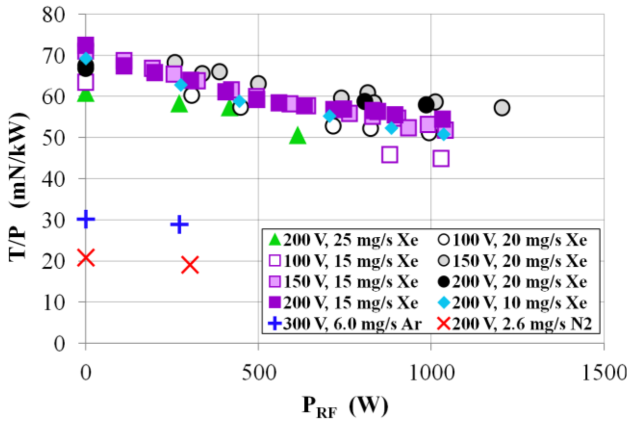


**Figure 9. Two-stage thrust-to-power, including both $P_d$ and $P_{rf}$, versus rf power.**

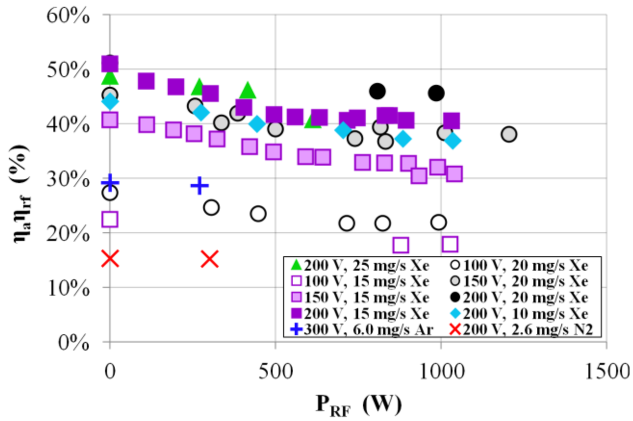


**Figure 10. Total anode efficiency versus rf power.**

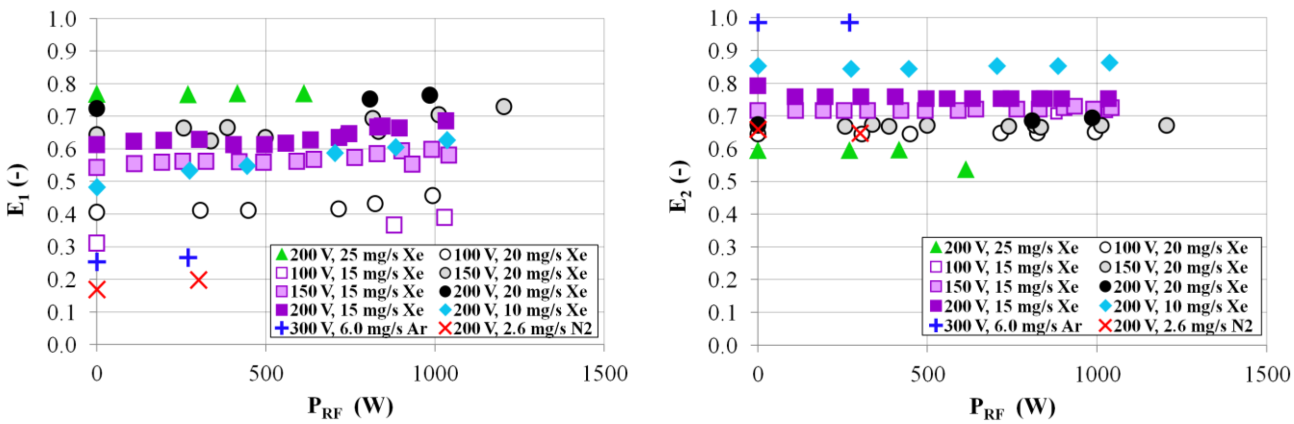


**(a)** **(b)**

**Figure 11. Anode exchange parameters versus rf power.**

Because rf efficiency is defined separately from anode efficiency, the exchange parameters can be used to investigate how the rf power affects the overall thruster behavior. The exchange parameters are plotted against rf power in Fig. 11. Figure 11(a) shows that $E_1$ increases slightly with rf power. The trend decreases with increasing anode mass flow rate for xenon operating conditions, with rf power having no effect on $E_1$ for the 25-mg/s xenon

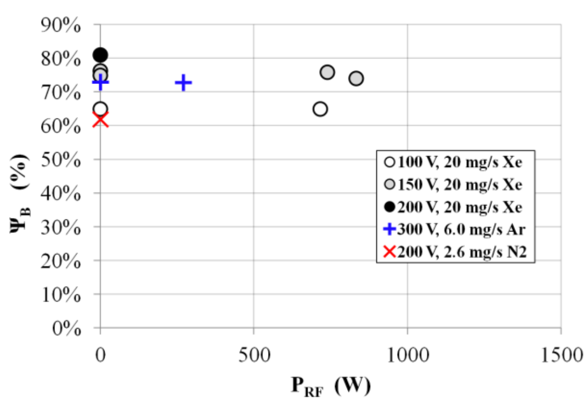


**Figure 12. Beam divergence efficiency versus rf power.**

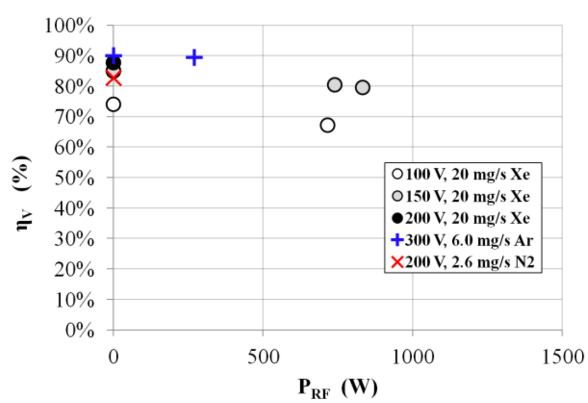


**Figure 13. Voltage utilization versus rf power.**

conditions. Only one operating point each for argon and nitrogen with rf power were performed, but both showed an increase in $E_1$. Current utilization, which is equal to $E_2$, is not significantly affected by rf power, as shown in Fig. 11(b), except that there is a sudden drop for the 25-mg/s xenon operating point at about 600 W.

Faraday probe results plotted in Fig. 12 show that rf power has no significant effect on beam divergence efficiency for the conditions that were measured. Figure 13 plots voltage utilization efficiency as a function of rf power, and shows a somewhat surprising result that voltage utilization tends to decrease with increasing rf power. The probe results together with Fig. 11 indicate that the rf power indeed increased propellant utilization efficiency, at least for the argon operating condition and for the 20-mg/s xenon operating conditions at 100 V and 150 V.

## V. Conclusion

The performance of the HHT operating in both single-stage and two-stage modes with argon, nitrogen, and xenon propellant was measured at the University of Michigan. Faraday probe, RPA, and Langmuir probe measurements in the far-field plume characterized the HHT beam divergence efficiency and voltage utilization. Beam divergence efficiency for nitrogen and argon propellant is lower than that expected for xenon at an equivalent discharge voltage and anode mass flow rate. Voltage utilization for argon and nitrogen is not significantly reduced, and so it is deduced that propellant utilization efficiency is also lower than that for xenon. Current utilization is a major source of anode inefficiency for nitrogen propellant, but not for argon. During two-stage operation, thrust is observed to increase slightly with rf power except at the 25-mg/s xenon propellant operating condition; however, thrust-to-power and total anode efficiency both consistently decrease with increasing rf power. The exchange parameters taken with limited probe results indicate that propellant utilization likely increases with rf power, but the increase is not sufficient to overcome the reduced efficiency due to the use of rf power.

## Acknowledgments

This work was performed by ElectroDynamic Applications as part of the Small Business Innovative Research (SBIR) program, under Air Force Contract FA9300-08-C-1007. The authors would like to acknowledge their partners at Aerojet, Andy Hoskins and Rafael Martinez. A. Shabshelowitz would also like to thank Dr. Alex Kiekhafer and Prof. Mitchell Walker of Georgia Tech for their helpful discussions regarding EMI, and Anthony Sebastion from the Lurie Nanofabrication Facility at the University of Michigan for his advice regarding rf hardware.

## References

[1]Hofer, R.R., “Development and Characterization of a High-Efficiency, High-Specific Impulse Xenon Hall Thruster,” Ph.D. Dissertation, Dept. of Aerospace Engineering, University of Michigan, Ann Arbor, MI, 2004.

[2]Mikellides, I.G., Katz, I., Hofer, R.R., Goebel, D.M., de Grys, K., and Mathers, A., “Magnetic Shielding of the Acceleration Channel Walls in a Long-Life Hall Thruster,” AIAA-2010-6942, *46th AIAA/ASME/SAE/ASEE Joint Propulsion Conference & Exhibit*, Nashville, TN, July 2010.

[3]Makela. J.M., Washeleski, R.L., Massey, D.R., King, L.B., and Hopkins, M.A., “Development of a Magnesium and Zinc Hall-effect Thruster,” IEPC-2009-107, *31st Ineternational Electric Propulsion Conference*, Ann Arbor, MI, September 2009.

[4]Szabo, J., Robin, M., Duggan, J., and Hofer, R.R., “Light Metal Propellant Hall Thrusters,” IEPC-2009-138, *31st International Electric Propulsion Conference*, Ann Arbor, MI, September 2009.

[5]Liang, R., and Gallimore, A.D., “Constant-Power Performance and Plume Properties of a Nested-Channel Hall-Effect Thruster,” IEPC-2011-030, *32nd International Electric Propulsion Conference*, Wiesbaden, Germany, September 2011.

[6]Florenz, R., Gallimore, A., and Peterson, P., “Developmental Status of a 100-kW Class Laboratory Nested Channel Hall Thruster,” IEPC-2011-246, *32nd International Electric Propulsion Conference*, Wiesbaden, Germany, September 2011.

[7]Martinez, R.A., Hoskins, W.A., Peterson, P.Y., and Massey, D., “Development Status of the Helicon Hall Thruster,” IEPC-2009-120, *31st International Electric Propulsion Conference*, Ann Arbor, MI, September 2009.

[8]Kamhawi, H., Manzella, D., Pinero, L., Haag, T., Mathers, A., and Liles, H., “In-Space Propulsion High Voltage Hall Accelerator Development Project Overview,” AIAA 2009-5282, *45th AIAA/ASME/SAE/ASEE Joint Propulsion Conference*,

[9]Boswell, R.W., and Chen, F.F., “Helicons – The Early Years,” *IEEE Transactions on Plasma Science*, Vol. 25, No. 6, December 1997, pp. 1229-1244. doi: 10.1109/27.650898

[10]Chen, F.F., and Boswell, R.W., “Helicons – The Past Decade,” *IEEE Transactions on Plasma Science*, Vol. 25, No. 6, Decemeber 1997, pp. 1245-1257. doi: 10.1109/27.650899

[11]Pottinger, S., Lappas, V., Charles, C., and Boswell, R., “Performance characterization of a double layer thruster using direct thrust measurements,” *Journal of Applied Physics D: Applied Physics*, Vol. 44, No. 23, June 2011.
doi: 10.1088/0022-3727/44/23/235201

[12]Shabshelowitz, A., and Gallimore, A.D., “Divergence Angle of Ion Beams Emanating from an Immersed Radiofrequency Plasma Source,” IEPC-2011-166, *32nd International Electric Propulsion Conference*, Wiesbaden, Germany, September 2011.

[13]Palmer, D., Walker, M.L.R., Manente, M., Carlsson, J., Bramanti, C., and Pavarin, D., "Performance Analysis of a Low-Power Helicon Thruster," AIAA-2008-4925, *44th Joint Propulsion Conference*, Hartford, CT, July 2008.

[14]Pavarin, D., et al., "Design of a 50 W Helicon Plasma Thruster," IEPC-2009-205, *31st International Electric Propulsion Conference*, Ann Arbor, MI, September 2009.

[15]Longmier, B.W., et al., "VX-200 Magnetoplasma Performance Results Exceeding Fifty-Percent Thruster Efficiency," *Journal of Propulsion and Power*, Vol. 27, No. 4, July-August 2011, pp. 915-920. doi: 10.2514/1.B34085

[16]Nakamura, T., et al., "Experimental Investigation of Plasma Acceleration by Rotating Electric Field for Electrodeless Plasma Thruster," IEPC-2011-279, *32nd International Electric Propulsion Conference*, Wiesbaden, Germany, September 2011.

[17]Slough, J., Kirtley, D., and Weber, T., "Pulsed Plasmoid Propulsion: The ELF Thruster," IEPC-2009-265, *31st International Electric Propulsion Conference*, Ann Arbor, MI, September 2009.

[18]Palmer, D.D., and Walker, M.L.R., "Operation of an Annular Helicon Plasma Source," *Journal of Propulsion and Power*, Vol. 25, No. 5, September-October 2009, pp. 1013-1019. doi: 10.2514/1.41403

[19]Peterson, P.Y., Massey, D.R., Shabshelowitz, A., Shastry, R., and Liang, R., "Performance and Plume Characterization of a Helicon Hall Thruster," IEPC-2011-269, *32nd International Electric Propulsion Conference*, Wiesbaden, Germany, September 2011.

[20]Brown, D.L., Larson, C.W., Beal, B.E., and Gallimore, A.D., "Methodology and Historical Perspective of a Hall Thruster Efficiency Analysis," *Journal of Propulsion and Power*, Vol. 25, No. 6, November-December 2009, pp. 1163-1177. doi: 10.2514/1.38092

[21]Liang, R., and Gallimore, A.D., "Far-Field Plume Measurements of a Nested-Channel Hall-Effect Thruster," AIAA-2011-1016, *49th AIAA Aerospace Sciences Meeting*, Orlando, FL, January 2011.

[22]Xu, K., and Walker, M.L.R., "High-Power, Null-Type, Inverted Pendulum Thrust Stand," *Review of Scientific Instruments*, Vol. 80, No. 5, May 2009. doi: 10.1063/1.3125626

[23]Kieckhafer, A.W., and Walker, M.L.R., "RF Power System for Thrust Measurements of a Helicon Plasma Source," *Review of Scientific Instruments*, Vol. 81, No. 7, July 2010. doi: 10.1063/1.3460263

[24]Brown, D.L, and Gallimore, A.D., "Evaluation of ion collection area in Faraday probes," *Review of Scientific Instruments*, Vol. 81, No. 6, June 2010. doi:10.1063/1.3449541

[25]Brown, D.L., "Investigation of Low Discharge Voltage Hall Thruster Characteristics and Evaluation of Loss Mechanisms," Ph.D. Dissertation, Dept. of Aerospace Engineering, University of Michigan, Ann Arbor, MI, 2009.

[26]Lemmer, K.M., "Use of a Helicon Source for Development of a Re-Entry Blackout Amelioration System," Ph.D. Dissertation, Dept. of Aerospace Engineering, University of Michigan, Ann Arbor, MI, 2009.

[27]Linnell, J.A., "An Evaluation of Krypton Propellant in Hall Thrusters," Ph.D. Dissertation, Dept. of Aerospace Engineering, University of Michigan, Ann Arbor, MI, 2007.

[28]Lias, S.G., "Ionization Energy Evaluation" in *NIST Chemistry WebBook, NIST Standard Reference Database Number 69*, Eds. P.J. Linstrom and W.G. Mallard, National Institute of Standards and Technology, Gaithersburg, MD, 20899, http://webbook.nist.gov, retrieved May 31, 2012.